Train wheel diagnostics by laser ultrasonics

TRAIN WHEEL DIAGNOSTICS BY LASER ULTRASONICS

Alfonso Cavuto, Milena Martarelli, Giuseppe Pandarese, Gian Marco Revel, Enrico Primo Tomasini

Original publication available at:

10.1016/j.measurement.2015.11.014

Highlights

- Study of different configurations of laser-ultrasonics for the inspection of wheels by a FE model.
- The carrying out of an experiment on a real train wheel.
- The FE model allowed identifying the optimal position of the air-coupled US probe.
- Experimental and simulated data are clearly correlated.
- The experimental tests were able to identify the presence of simulated defects on the train wheel.

TRAIN WHEEL DIAGNOSTICS BY LASER ULTRASONICS

A. Cavuto[a*], M. Martarelli[b], G. Pandarese[a], G.M. Revel[a], E.P. Tomasini[a]

a. Università Politecnica delle Marche, Via Brecce Bianche, Ancona

b. Università degli Studi e-Campus, Via Isimbardi, Novedrate (CO)

Corresponding author: a.cavuto@univpm.it

DIISM, Università Politecnica delle Marche, Ancona, Italy

Abstract

The integrity of the wheel is very important for the safety of railway. In this paper a laser-ultrasonic diagnostic measurement procedure has been designed for the inspection of the train wheels with the aid of a FE-model simulating the ultrasound propagation within the wheel itself.

The laser-ultrasonic method exploits an air-coupled ultrasonic probe that detects the ultrasonic waves generated by a high-power pulsed laser. As a result, the measurement chain is completely non-contact, from generation to detection, this making it possible to considerably speed up inspection time and make the set-up more flexible. The main advantage of the technique developed is that it works in thermo-elastic regime and it therefore can be considered as a non-destructive method.

The diagnostic procedure developed has been applied for the inspection of train wheels provided by the Italian railway company Trenitalia, on which dominant wheel failure cracks have been expressly created.

Keywords: Laser-ultrasonics, NDT, air-coupled ultrasound, train wheels, FE model

1. Introduction

Safety and reliability are two key issues in the railway field. Wheelset components, i.e. axle and wheels, are often the main responsible for breakdowns and accidents, they being most subjected either to static stress or fatigue. In particular, the wheels are subjected to heavy loads caused by the rail-wheel contact [1, 2], this generating many different types of defects [3].

Although the railway components are designed for unlimited life, they occasionally collapse during operation because of the propagation of incipient cracks. Therefore their periodic inspection is crucial. An open problem is, however, the estimation of the optimal inspection frequency intervals (according to the concept of damage tolerance) so as to increase safety without shortening the periods between controls [4], this making it possible to reduce maintenance costs. Currently the inspection of wheel is carried out by ultrasonic techniques, i.e. phased arrays which are employed during periodical inspections or after re-profiling [5, 6, 7, 8].

Ultrasonic techniques, which are well known in the state of the art, have the disadvantage of requiring the probes to be in contact with the object to be investigated, which lengthens the inspection time necessary to prepare the object and apply the coupling medium. In case of highly automated systems, the equipment is complex and expensive; often several phased array are necessary to inspect each part of the wheel. Those typical problems of conventional ultrasonic techniques can be overcome by using a hybrid laser-ultrasonic system based on the detection of ultrasonic waves generated by a high-power pulsed laser via air-coupled ultrasonic transducers [9]. Air-coupled ultrasound inspection has already been successfully used in many industrial applications e.g. NDT on both thick [10] and thin [11] composites, NDT on light thin historical vaults [12], density measurement of ceramic tiles [13], wood detection [14], and thin metallic laminated [15, 16].

The hybrid system here proposed is completely non-invasive and it makes it possible to:

- overcome shape and accessibility problems,
- avoid the application of the coupling medium,

- shorten the inspection time for large surfaces.

Laser-ultrasonics has been applied in different fields for defects detection, in the aeronautical field for damage detection on thick composite materials [17] and honeycombs [18], in the railway field for rail [19, 20], rail wheels [9] and axle inspection [21] and in metal slabs production [22]. Kenderian et al. [9] presented a Laser Air-Hybrid Ultrasonic Technique based on air-coupled ultrasounds. The main limitation of the technique is due to the fact that it works in ablative regime to generate guided waves and thus the surface is damaged and the method cannot be considered non-destructive. The use of guided waves allows detecting only superficial defects, which are not the only existing in wheels. In a very recent work the authors have proposed a laser-ultrasonic technique that works in thermo-elastic regime for the inspection of train axle superficial defects with promising results [23]. In that case, ultrasonic surface waves have been exploited for the diagnostics of the defects. In this paper, the same ultrasonic procedure based on thermo-elastic wave propagation has been applied but bulk waves have been exploited since the identification of in-depth defects is now tackled. Moreover, the geometrical complexity of the wheel makes difficult the interpretation of the surface wave's propagation for diagnostic purposes. The inspected train wheel has been supplied by the Italian railway company (Trenitalia), where dominant wheel failure cracks have been expressly created [24] according to defects occurring in real wheelset [3]. The experimental procedure has been driven by numerical simulations based on a FE model of the generation and the propagation of the ultrasonic waves within the wheel material.

The paper is structured in four Sections. Section 2 presents the FE model developed for the design of the experimental measurement procedure and, in practice, to identify the optimal laser source and ultrasonic probe positions before performing the test. The numerical FE model simulates the generation of the thermo-elastic displacement by a high-power pulsed laser impinging on the material surface and the propagation of the ultrasonic wave produced by the thermo-elastic effect within the material. The simulation allows to identify the propagation paths of the different

propagation modes and therefore to estimate the relative position of laser source and receiving probe in which the SNR (Signal to Noise Level) will be optimal. The experimental set-up is reported in Section 3, and the results obtained in the tests are discussed in Section 4.

2. Design of experimental measurement procedure based on numerical FE model

A coupled thermo-stress analysis was exploited to simulate the generation and the propagation of elastic waves and to drive the experiments by identifying the probe position and inspection parameters.

2.1. Simulation of the elastic wave propagation on a 2D wheel section

In laser ultrasonics the ultrasonic waves are generated by a high power pulsed laser impinging on the surface of the material under test. Two different physics need to be considered to simulate the ultrasonic phenomenon: thermo-elasticity, for the ultrasonic wave generation due to the thermo-stress induced by the laser impulse [25, 26], and acoustics, for the ultrasonic wave propagation within the material [27]. Comsol Multiphysics software was used to carry out the numerical simulation. The FE model developed has been validated on both a simplified test item [28] and on a portion of a train axle [23].The propagation of the elastic waves was modeled following the thermal diffusion and thermo-elastic displacement equations [27]:

$$\rho C \frac{\partial T}{\partial t} - \nabla(k \nabla T) = Q \tag{1}$$

$$(\lambda + \mu)\nabla(\nabla \boldsymbol{u}_1) - \mu \nabla \times \nabla \times \boldsymbol{u}_1 - \rho \frac{\partial^2 \boldsymbol{u}_1}{\partial t^2} = \alpha(3\lambda + 2\mu)\nabla T \tag{2}$$

where T is the temperature rise in the metal, k is the thermal conduction coefficient, ρ is the density, C is the constant specific heat, Q is the heat source created by laser irradiation, α is the linear thermal expansion coefficient, λ and μ are the Lamé constants and $\boldsymbol{u_1}$ is the displacement vector due to the thermo-elastic effect.

The elastic wave equation is obtained from Newton's second law:

$$\rho \frac{\partial^2 \boldsymbol{u_2}}{\partial t^2} - \nabla \boldsymbol{s} = \boldsymbol{F}_v \tag{3}$$

where $\boldsymbol{u_2}$ is the displacement vector due to the elastic effect, $\boldsymbol{s}$ is the stress tensor and $\boldsymbol{F_v}$ represents the volume force vector. To study the wave's propagation, considering the superficial (Rayleigh) wave frequency components up to 1 MHz (f) the shortest wavelength is:

$$\lambda_r = \frac{c_r}{f} = \frac{3000 \cdot 10^3}{1 \cdot 10^6} = 30\ mm \tag{4}$$

The Rayleigh velocity (c_r) was measured experimentally, it resulting in 3000 m/s.

A 2D wheel section was simulated with a free triangular mesh. The size of the finite elements was chosen in order to have a suitable spatial resolution of the propagating waves. It is recommended [29, 30] to have at least 10 nodes per wavelength and therefore the element size must be at least 1/10 of the shortest wavelength to be analyzed, i.e. smaller than $l_e=\lambda_r/10=0.3\ mm$, where λ_r is the Rayleigh wavelength.

The model made it possible to simulate the propagation of the elastic wave within the wheel section and to verify the paths of the bulk waves and the interaction with the wheel profile, as illustrated in Fig. 1 where the instantaneous total displacement at three consequent instants are plotted.

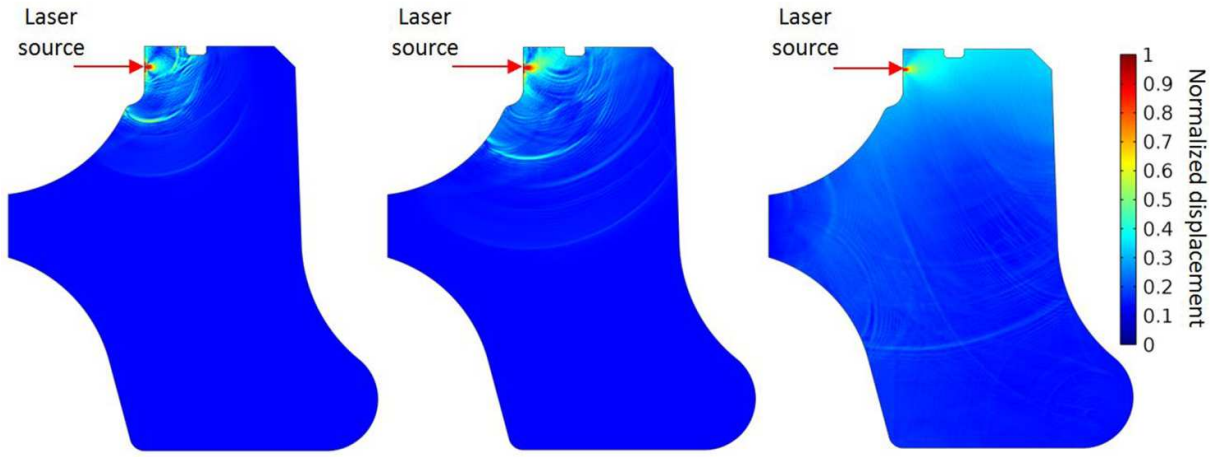

Fig. 1 Elastic wave's propagation: a) at 6 µs, b) at 10 µs; c) at31 µs. The laser source position is on the top left of the wheel section and it is marked with the arrow.

2.2 FE model exploitation for test planning

As evidenced in Fig.1, the FE model allows identifying the most energetic paths of the elastic waves generated by the laser source and propagating within the wheel section geometry. The directivity pattern of such waves can be plotted in polar coordinates, as in Fig.2. For both the longitudinal (P-wave) and shear (S-wave) waves the total displacement amplitude has been evaluated in correspondence of the bulk wave position (red semicircles) reached at the time instant of 3 μs for the P-wave and 6 μs for the S-wave. The directivity of the longitudinal (P-wave) and shear (S-wave) waves shows a preferential direction of propagation at 30 deg for the S-wave and at 60 deg for the P-wave in according with the thermo-elasticity theory [31].

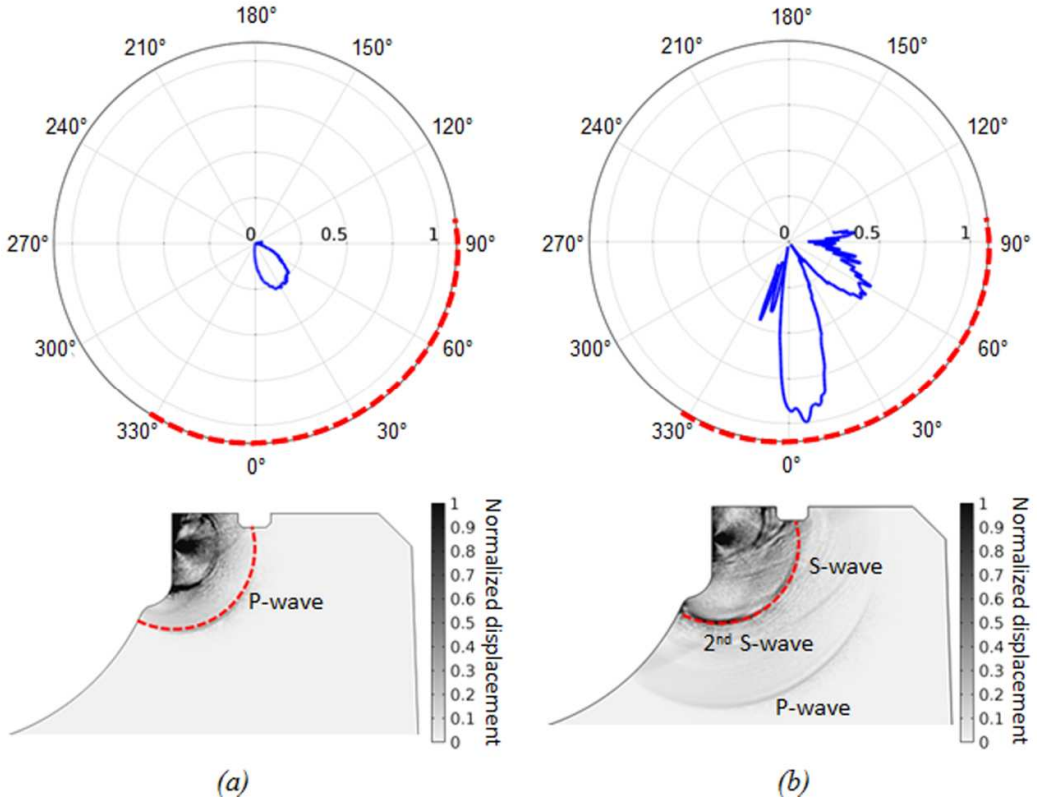

Fig. 2 a) P-wave polar diagram, at 3 μs; b) S-waves polar diagram, at 6 μs.

It can be noticed that at the same position in space the S-wave is more energetic than the P-wave and this fact induced to use as propagation mode for the defect diagnostic the S-wave. In addition,

another important contribution can be noticed in the S-wave polar diagram which is due to a secondary S-wave detached from the surface wave when it encounters the section variation. Those waves are also illustrated in the wheel section propagation path shown in Fig. 3a. A similar analysis can be done on the wheel profile in order to identify the area where the elastic waves are more energetic and therefore the ultrasonic signal has a higher SNR. When observing a typical ultrasonic signal simulated on the wheel profile, as the one of Fig. 3b, the different elastic wave's time of arrivals can be distinguished. If a RMS is calculated on a time window of 10 µs centered at around the time of arrival of the S-wave (see Fig. 3b) and this is repeated for different positions, from 1 to 16, as reported in Fig. 3a, the RMS profile can be drawn for the entire wheel contour (see Fig. 3c).

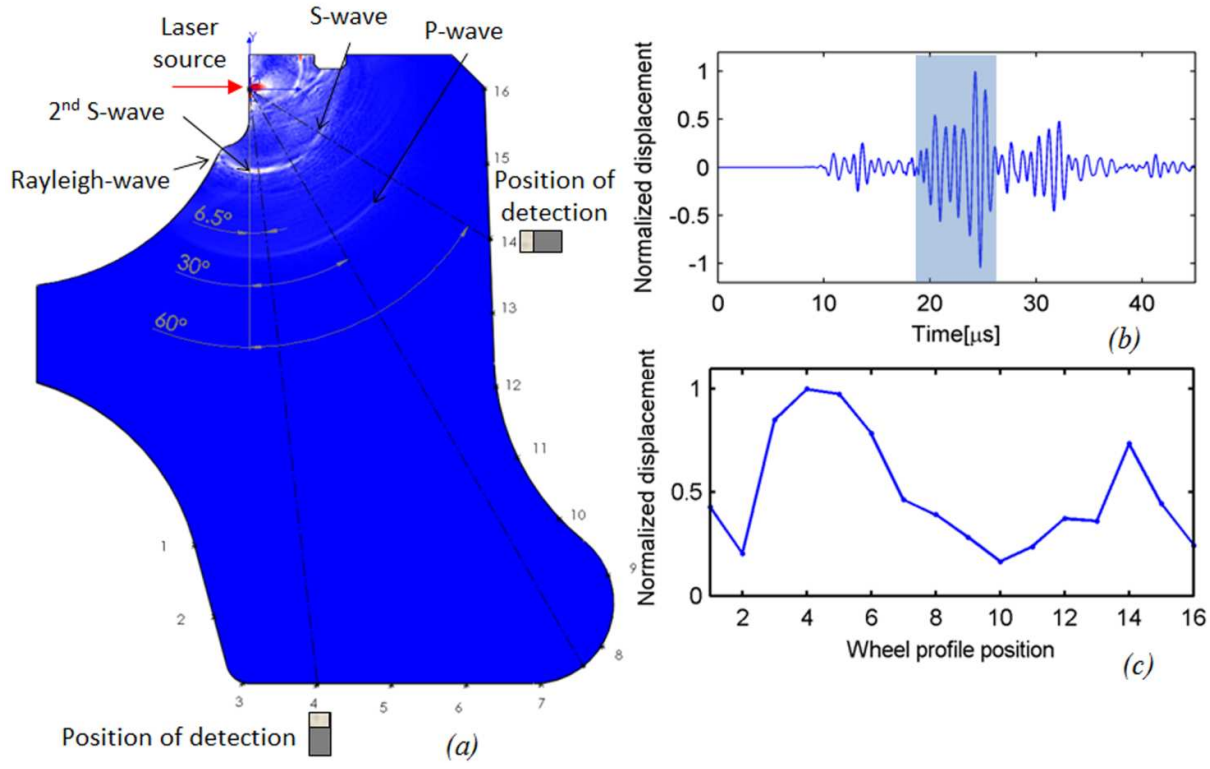

Fig. 3 a) Elastic wave patterns in the wheel material; b) Ultrasound total displacement on a generic point of the wheel profile with the time window used for the RMS calculation evidenced; c) RMS around the S-wave time of arrival (time windowed evidenced in b) on the set of positions in the wheel profile.

The RMS profile indicates that the maximum signal is in correspondence of the positions 4 and 14 which are therefore the optimal locations for a US probe to monitor the S-wave. This effect was expected from the polar plots of Fig. 2, but such kind of visualisation allows directly identifying the best position on the wheel surface in terms of higher SNR.

3. Experimental set-up

3.1. Test bench

The railway wheel inspected has been mounted over another identical wheel used as support by means of a dedicated bearing system that allows relative rotation. An encoder mounted on the wheel shaft measured the angular position of the wheel made to rotate by an electric motor. The probes were installed on a frame where they could move along the wheel axial and radial directions. Therefore, the laser ultrasonic system can inspect the complete tread of the wheel, see Fig. 4. A second configuration, as described in the next sections, allowed scanning the back face of the rim.

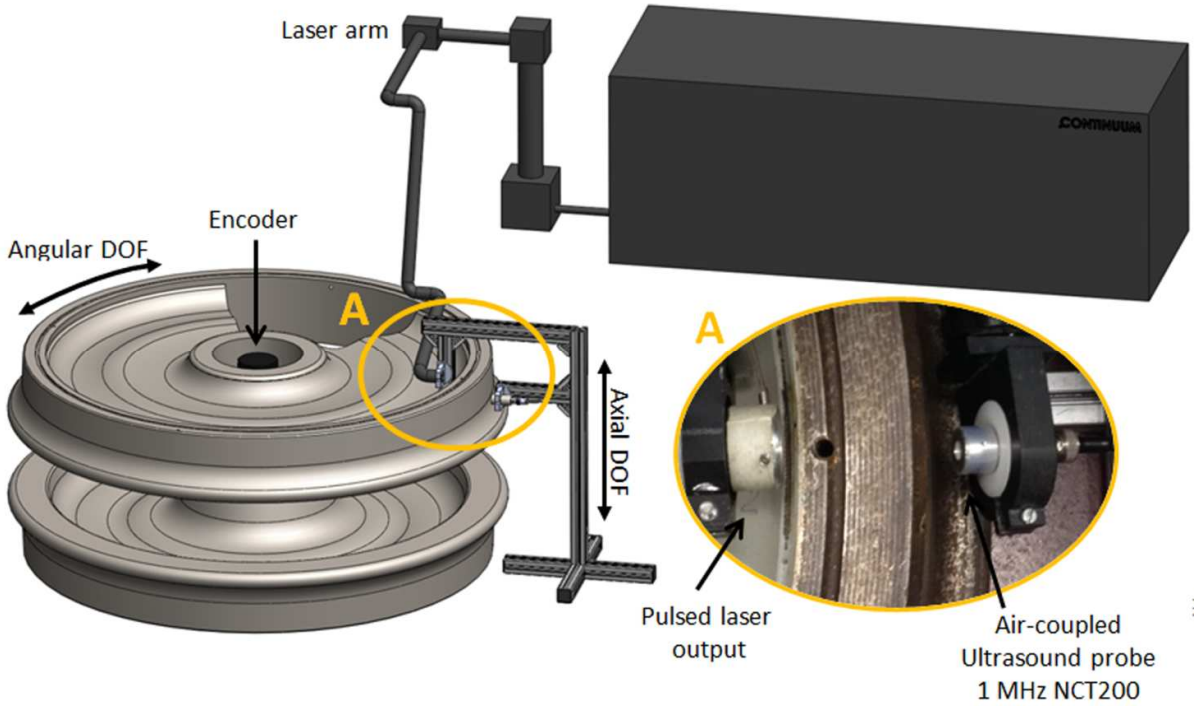

Fig. 4. The laser-ultrasonic experimental set-up.

The laser ultrasonic system was made up of a pulsed laser source, a Continuum Nd-Yag IR laser (1064 nm) with pulses of 12 ns duration and 82 mJ energy and a 1 MHz air-coupled ultrasound piezoelectric probe by Ultran Group (model NCT210, with 8 mm diameter of active area). The ultrasound probe conditioning system was a DPR-300 Pulser/Receiver from JSR Ultrasonics. The ultrasound signals were amplified with a gain level of 69 dB and acquired with a high speed Digitizer board NI PXI-5122 (100 MHz bandwidth). The laser beam was guided towards the wheel under test by means of an arm connected to the pulsed laser cavity and pointed on the inside diameter of the rim as shown in Fig. 4. A collimated laser beam with a diameter of about 8.5 mm was used to keep the ultrasonic waves generation within a thermo-elastic regime. The air-coupled ultrasound probe was placed in two positions defined on the basis of the model results that indicated positions 4 and 14 as the optimal ones in terms of highest SNR.

A circumferential scan was performed along an angle of 8 deg with an angular resolution of 0.25 deg.

3.2. Test item

The test item is a train wheel, Fig. 5, on which typical fatigue defects were created. Such kind of defects caused by external damage or during the manufacturing process could thereafter propagate caused by repeated contact stress between the wheel and the rail during rolling motion. In practice, a radial defect was simulated with a 7 mm diameter flat-bottom hole generated perpendicular to the rim face, to a depth of 90 mm and with the axis at a distance of 10 mm from the inside diameter of the rim (Fig. 6). Furthermore a circumferential defect (Fig. 6) was simulated with a 7 mm diameter flat-bottom hole generate parallel to the rim face, to a depth of 25 mm.

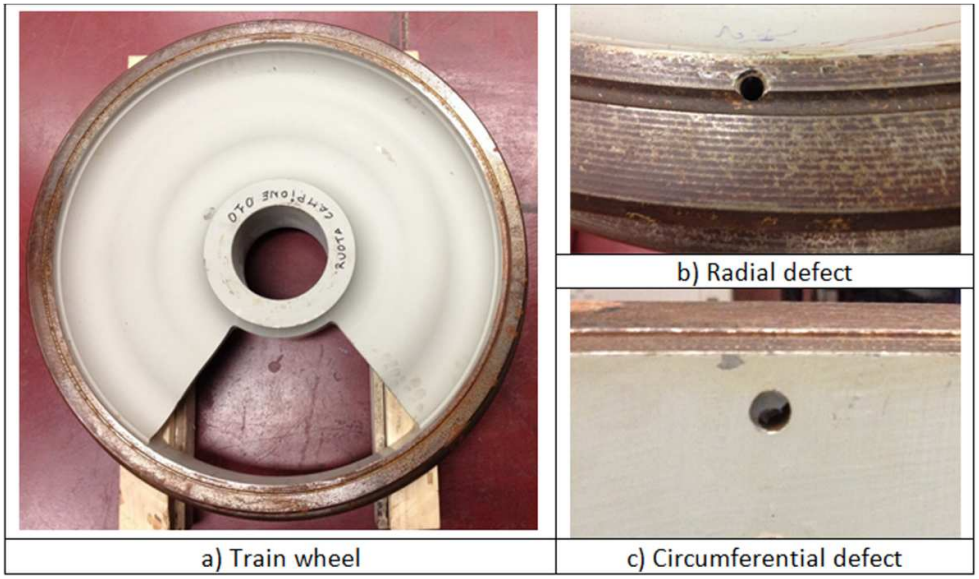

Fig.5. Test item (a) and defects created on it (b and c)

4. Analysis of results

Fig.4 shows the experimental configurations realized for the radial and circumferential defects diagnostics. Following the nomenclature given to the probe positions in Fig. 3a, the radial defect was monitored from the positions 4 and 14, the circumferential one from the position 14 (Fig. 6). A preliminary test allowed confirming that the S-wave is the most efficient propagation mode as predicted by the FE model (see the polar diagrams of Fig. 2). The probe axis was tilted with respect to the surface normal of 6 deg, according to Snell's law [32], which is the optimal angle for the detection of the S-wave. The laser source was pointed on the outer edge of the wheel for both the defect types.

4.1 Experimental vs FE model results

First, a comparison between the experimental and the numerical results has been done in correspondence to the measurement points number 4 and 14. The waveforms measured experimentally have been shifted in time of 41 μs for both the points numbers 4 and 14 due to the air path traveled by the ultrasonic waves, being the US probe coupled in air.

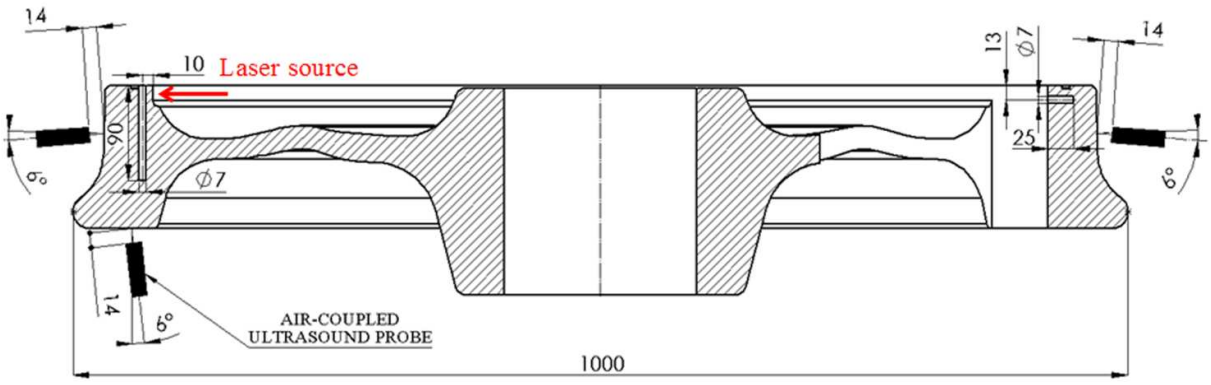

Fig. 6. US probe configuration and defect positions: radial defect on the left, axial defect on the right; size are in mm.

In Fig. 7 and 8 the time histories measured and simulated in the locations 4 and 14, respectively, are reported. Experimental and simulated data are clearly correlated; the P- and S-waves are aligned, thus confirming the model consistency.

Discrepancies may be due to:

- transfer function of air-coupled ultrasound probe;
- dimension of the active area of the ultrasound probe;
- elastic waves propagation through the air domain;
- different acoustic impedance between the interfaces wheel-air and air-active area of the probe.

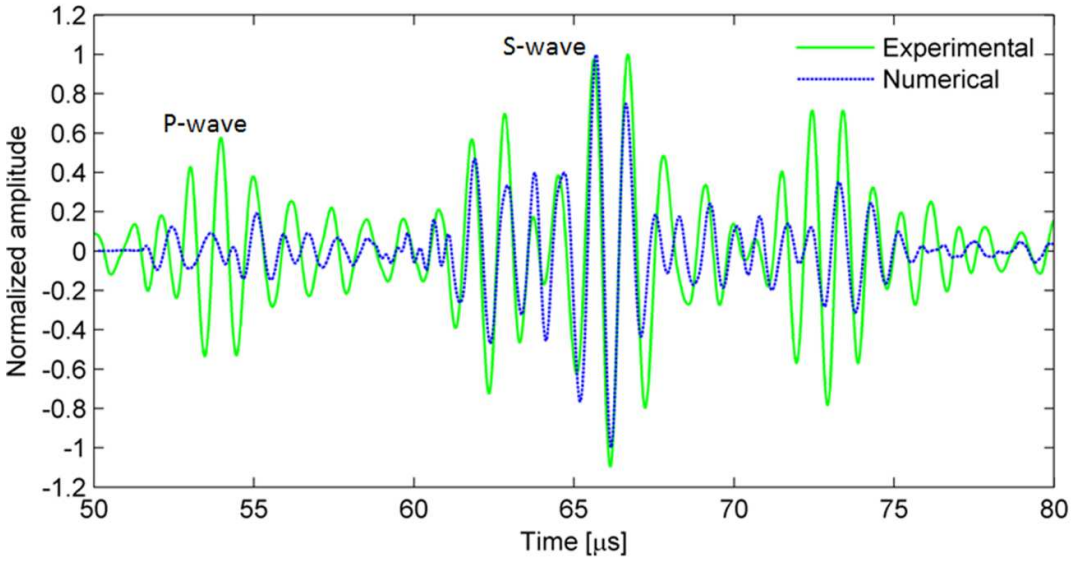

Fig. 7. Superposition of experimental (green line) and simulated time history (blue line) in the position 14.

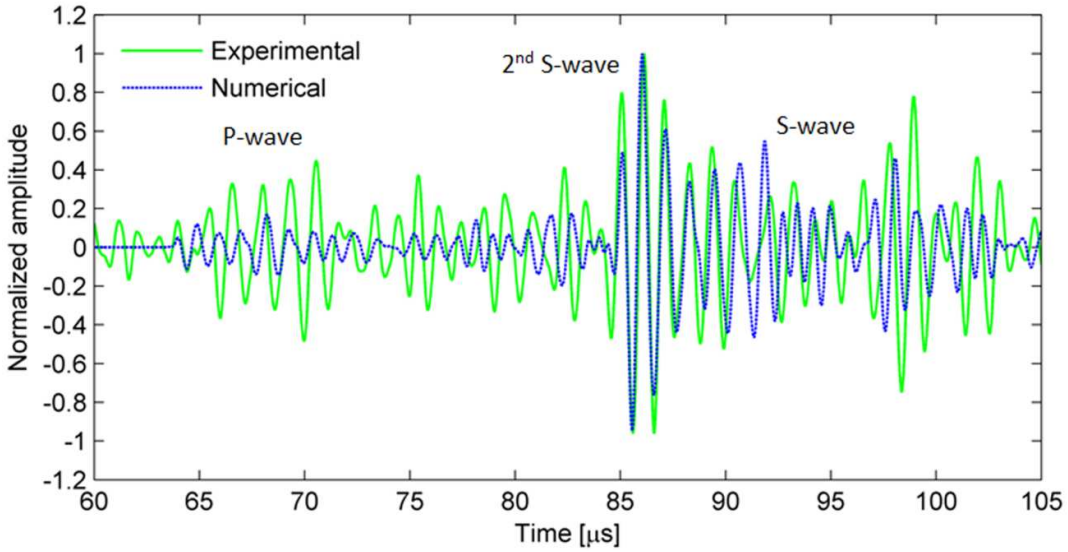

Fig. 8. Superposition of experimental (green line) and simulated time history (blue line) in the position 4.

4.2 Defects diagnostics

4.2.1 Radial defect

The identification of the defects was performed by scanning 33 points along the arc of 8 deg on the wheel profile. The time histories recorded in each points were considered in a time window of 15 μs

around the S-Wave time of arrival and plotted together in the form of a B-scan, it having the time and the angular position in the x- and y-axis respectively.

Fig. 9a left, shows the B-scan obtained when the US probe was located in the position 14, while Fig. 9a right, the B-scan obtained when the US probe was located in the position 4. The occurrence of the defect is evidenced by an attenuation of the S-wave because the waves pass through interfaces and a medium with different impedance. Fig. 9b reports the RMS plots obtained calculating the RMS value of each 33 time histories. Those plots confirm that the S-wave waves experienced a strong attenuation when passing through the defect.

The attenuation has been measured as the contrast between the RMS in the damaged and in the undamaged areas. The RMS contrast is of 7.8 dB when the US probe is located in point 4 and 7.7 in the point 14.

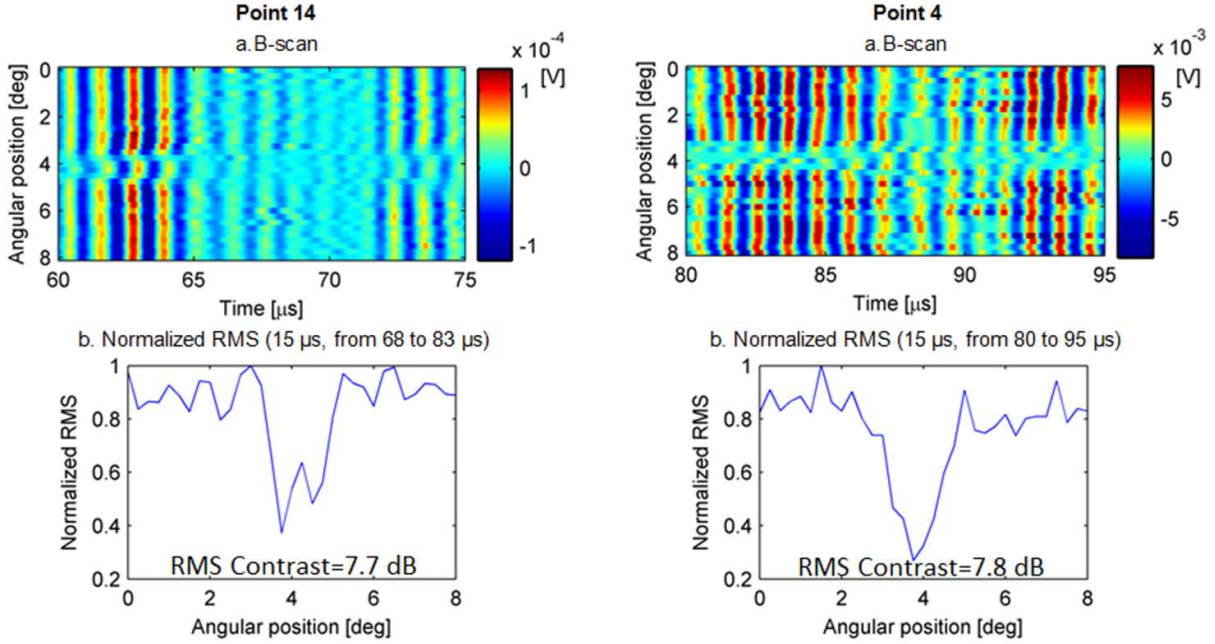

Fig. 9. Left: US probe in point 14, left column (a), B-scan (b) Normalized RMS in function of the scanning angle; Right: US probe in point 4, (a) B-scan (b) Normalized RMS in function of the scanning angle.

4.2.2 Circumferential defects

Similar results, as the ones described for the radial defect, were obtained for the circumferential defect. The US probe was positioned in point 14. The B-scan centered on the S-wave time of arrival with a time window of 15 μs and its RMS is reported in Fig. 10. The defect attenuation is evident and it is of 8.7 dB in terms of RMS.

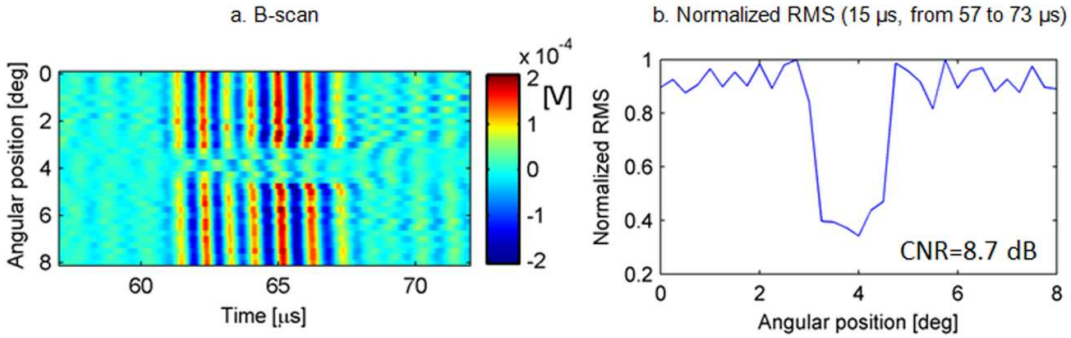

Fig. 10. US probe in point 14, B-scan (a), Normalized RMS in function of the scanning angle (b).

5. Conclusions

The paper has shown the applicability of laser-ultrasonics, a non-destructive, non-contact technique, for the inspection of train wheels. The main advantage of the proposed technique with respect to the state of the art is that it operates in thermo-elastic regime and therefore can be considered a non-destructive method. Furthermore, it is based on the fact that the defect produces an attenuation of the bulk waves, mainly the transversal one working in transmission mode.

Two typical wheel defects, radial and circumferential, have been considered in this work.

The experimental procedure was defined on the basis of the results of a multi-physics FE model that allowed identifying the optimal position of the air-coupled US probe. All the defects have been identified by observing the S-wave propagation, it presenting an evident attenuation (in the order of 7.8 dB) when passing through the damaged areas.

ACKNOWLEDGEMENTS

The authors wish to thank Trenitalia S.p.A. Direzione Tecnica - Ingegneria Rotabili e Tecnologie di Base and specifically Luca Labbadia and Marco Sarti for their precious contribution and for providing the train wheel. The work has been financed by the National Ministry of Education, University and Research within a National Project PRIN 2009PSJW8Z ‘‘Development of a laser-ultrasonic system for non-destructive-testing aiming at improving railway safety’’.

REFERENCES

[1] D. Milkovic , G. Simic, Z. Jakovljevic, J. Tanaskovic, V. Lucanin, Wayside system for wheel‑rail contact forces measurements, Measurement 46 (2013) 3308‑3318.

[2] H. Molatefi, H. Mozafari, Analysis of new method for vertical load measurement in the barycenter of the rail web by using FEM, Measurement 46 (2013) 2313‑2323.

[3] Railway applications - In-service wheelset operation requirements - In-service and off-vehicle wheelset maintenance, in EN 15313.

[4] L. Hajibabai, M. R. Saat, Y. Ouyan, C. P.L. Barka, Z. Yang, K. Bowlin, K. Soman, D. Lauro, X. Li, Wayside Defect Detector Data Mining to Predict Potential WILD Train Stops, in: Proceedings of the AREMA 2012 Annual Conference & Exposition, Chicago.

[5] J. Peng, L. Wang, The Design and Application of Lateral Phased Array Probe for Railway Wheel Rim Ultrasonic Detection System, in: Proceedings of the 18th WCNDT, South Africa, 2012.

[6] J. Peng, X. Gao, Y. Zhang, Z. Wang, C. Peng, Y. Tan, K. Yang, B. Zhao, An Ultrasonic technology Study for Subsurface Defect in Railway Wheel Tread, in: Proceedings of 11th European Conference on Non-Destructive Testing (ECNDT), Prague, Czech Republic, 2014.

[7] J. Peng, H. Peng, Y. Zhang, X. Gao, C. Peng, Z. Wang, Study on the railway wheel ultrasonic inspection method using the full matrix capture, Far East Forum on Nondestructive Evaluation/Testing: New Technology & Application (FENDT), Jinan, China, 2013.

[8] P.N. Marty, Latest Development in the UT inspection of train wheels and axles, in: Proceedings of 18th World Conference on Nondestructive Testing, Durban, South Africa, 2012.

[9] S. Kenderian, B. B Djordjevic, D. Cerniglia and G. Garcia, Dynamic railroad inspection using the laser-air hybrid ultrasonic technique, Insight 48 (6) (2006) 336-341.

[10] G.M. Revel, G. Pandarese, A. Cavuto, Advanced ultrasonic non destructive testing for damage detection on thick and curved composite elements for constructions, Journal of Sandwich structures and Material, 15(1) (2013) 1-20, DOI 10.1177/1099636212456861.

[11] P. Pietroni, G.M. Revel, Non contact ultrasonic techniques for composite material diagnostics in aeronautics applications, in: Proceeding of 9th European Conference on Non-Destructive Testing, Berlin, 2006.

[12] E. Quagliarini, G.M. Revel, S. Lenci, E. Seri, A. Cavuto, G. Pandarese, Historical plasters on light thin vaults: State of conservation assessment by a Hybrid ultrasonic method, Journal of Cultural Heritage 15 (2014) 104–111.

[13] G.M. Revel, Measurement of the apparent density of green ceramic tiles by a non-contact ultrasonic method, Experimental Mechanics 47(5) (2007) 637-48.

[14] M.R. Fleming, M. C. Bhardwaj, J. J. Janowiak, J.E. Shield, R. Roy, D.K. Agrawal, L. S. Bauer, D.L. Miller, K. Hoover, Noncontact ultrasound detection of exotic insects in wood packing materials, Forest Products Journal, June, 2005.

[15] D.W. Schindel, Air-coupled generation and detection of ultrasonic bulk waves in metals using micromachined capacitance transducers, Ultrasonics 35 (2) (1997) 179-181.

[16] W.M.D. Wright, D.A. Hutchins, Air-coupled ultrasonic testing of metals using broadband pulses in through-transmission, Ultrasonics 37 (1999) 19–22.

[17] D. Cerniglia, B.B. Djordjevic, V. Nigrelli, Quantitative subsurface defect detection in composite materials using a non-contact ultrasonic system, in: Proceedings of IEEE international Ultrasonics Symposium, Atlanta, 2001.

[18] C. Cosenza, D. Cerniglia, B.B. Djordjevic, Non-contact ultrasonic inspection of skin/core bond in honeycomb with Lamb waves, in: Proceedings of IEEE Ultrasonics Symposium, Monaco, 2002.

[19] S. Kenderian, B.B. Djordjevic, Jr. R.E. Green, Laser-based and air-coupled ultrasound as noncontact and remote techniques for testing railroad tracks, Materials Evaluation 60 (1) (2002) 65-70.

[20] D. Cerniglia, S. Kenderian, B.B. Djordjevic, G. Garcia, R. Morgan, Laser e trasduttore di accoppiamento in aria per l'ispezione ultrasonica non a contatto nel settore ferroviario, in: Proceedings of Conferenza AIPnD, Matera, Italy, 2002.

[21] K. Gonzales, S. Kendarian, D. Carter, A Smith, R Morgan, Non-contact interrogation of railroad axles using laser-based ultrasonic inspection, in: Proceedings of JRC2005, Pueblo, Colorado. DOI: 10.1109/RRCON.2005.186070.

[22] T. Mitter, H. Grün, J. Roither, A. Betz, S. Bozorgi B. Reitinge, P. Burgholzer, Detection and Reconstruction of Solidification Cracks -Laser Ultrasonic Measurements during the Continuous Casting Process of Aluminum, in: Proceedings of AIP Conference 2014; DOI: 10.1063/1.4879606.

[23] A. Cavuto, M. Martarelli, G. Pandarese, G.M. Revel, E.P. Tomasini, Experimental investigation by laser ultrasonics for high speed train axle diagnostics, Ultrasonics 55 (2015) 48–57.

[24] AAR Manual of Standards and Recommended Practices Wheels and Axles M-107/M-208.

[25] P. Castellini, G.M. Revel, L. Scalise, R.M. De Andrade, Experimental and numerical investigation on structural effects of laser pulses for modal parameter measurement, Optics and Lasers in Engineering 32(6) (2000) 565-581.

[26] P. Castellini, G.M. Revel, L. Scalise, Measurement of vibrational modal parameters using laser pulse excitation techniques, Measurement 35 (2004) 163-179.

[27] J. Wanga, Z. Shen, B. Xu, X. Ni, J. Guan, J. Lu, Numerical simulation of laser-generated ultrasound in non-metallic material by the finite element method, Optics & Laser Technology 39 (2007) 806–813.

[28] A. Cavuto, F. Sopranzetti, M. Martarelli, G.M. Revel, Laser-Ultrasonics Wave Generation and Propagation FE Model in Metallic Materials, in: Proceeding of COMSOL Conference, Rotterdam, 2013.

[29] D. Cerniglia, A. Pantano, C. Mineo, Influence of laser beam profile on the generation of ultrasonic waves, Appl. Phys. A. 105 (2011) 959–967.

[30] D. Alleyne, P. Cawley, A two-dimensional Fourier transform method for measurement of propagating multimode signals, Journal of the Acoustical Society of America 89 (3) (1991) 1159–68.

[31] C.B. Scruby, L.E. Drain, Laser Ultrasonics: Techniques and Applications, CRC Press, 1990.

[32] I. Solodov, D. Döring, G. Busse, Air-Coupled Lamb and Rayleigh Waves for Remote NDE of Defects and Material Elastic Properties, Journal of Mechanical Engineering 56 (9) (2010) 557-564.

Fig.1 Elastic wave's propagation

Click here to download high resolution image

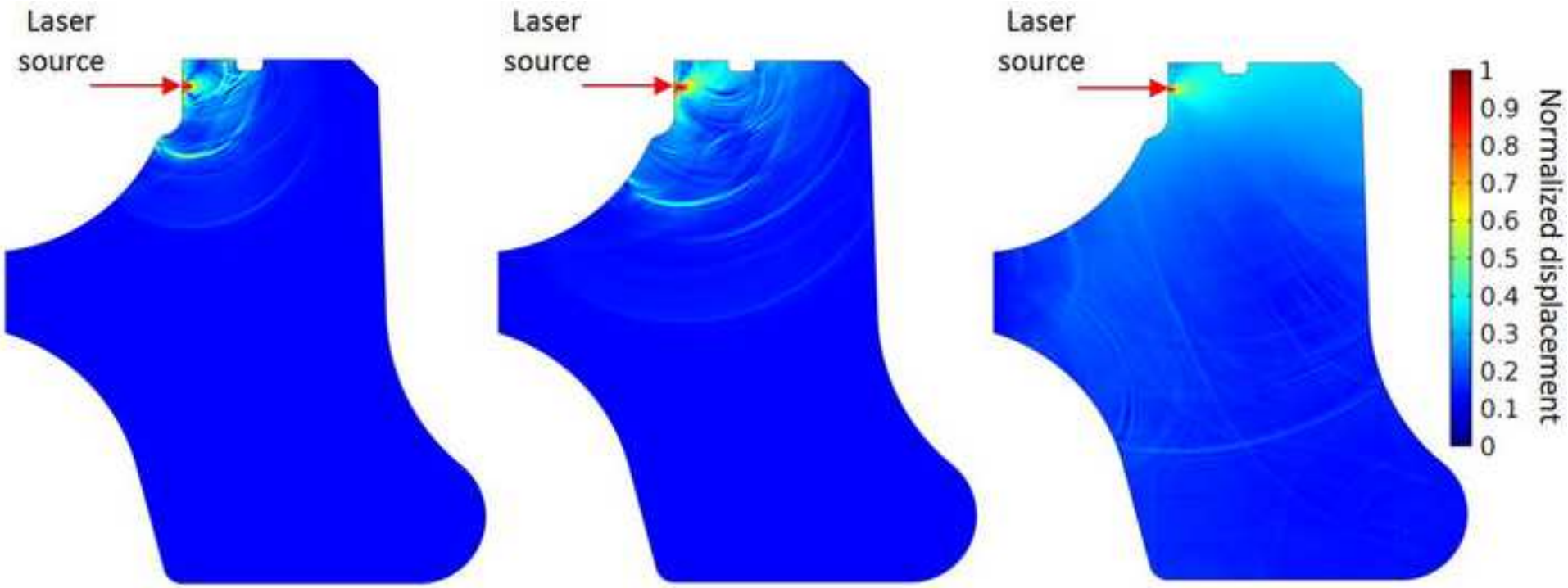

Fig. 2 a) P-wave polar diagram

Click here to download high resolution image

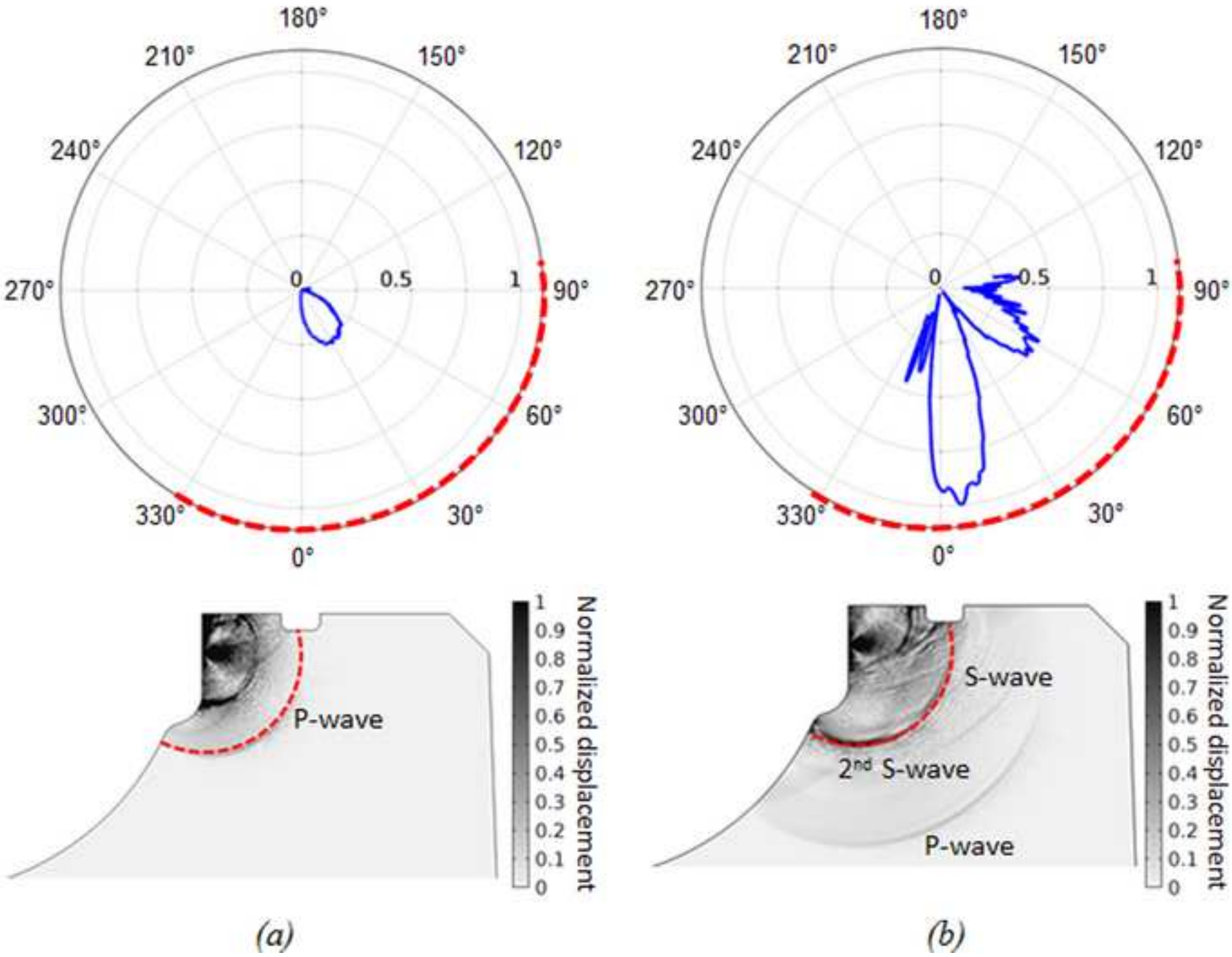

Fig. 3 a) Elastic wave patterns in the wheel material

Click here to download high resolution image

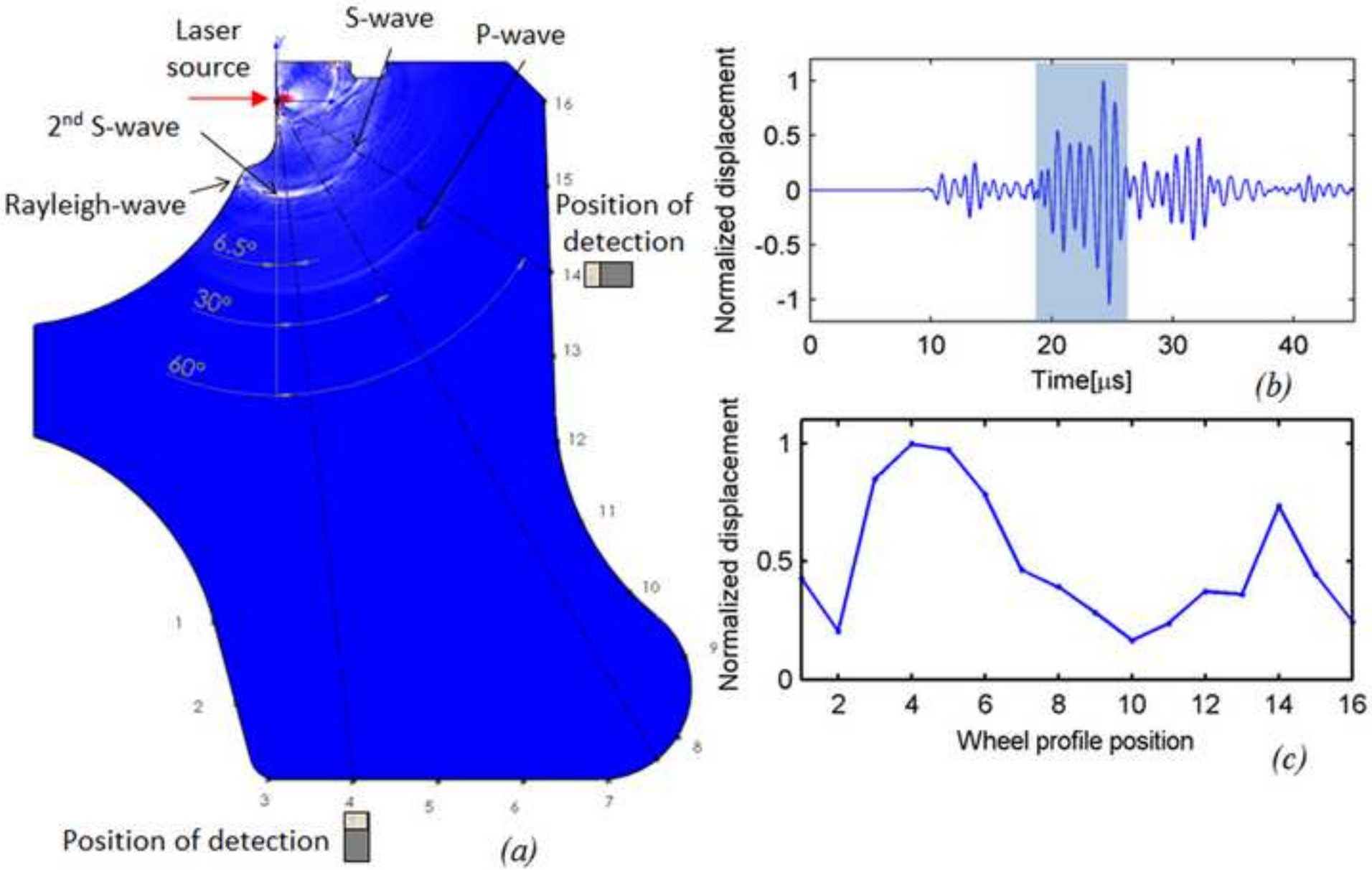

Fig. 4. The laser-ultrasonic experimental set-up
Click here to download high resolution image

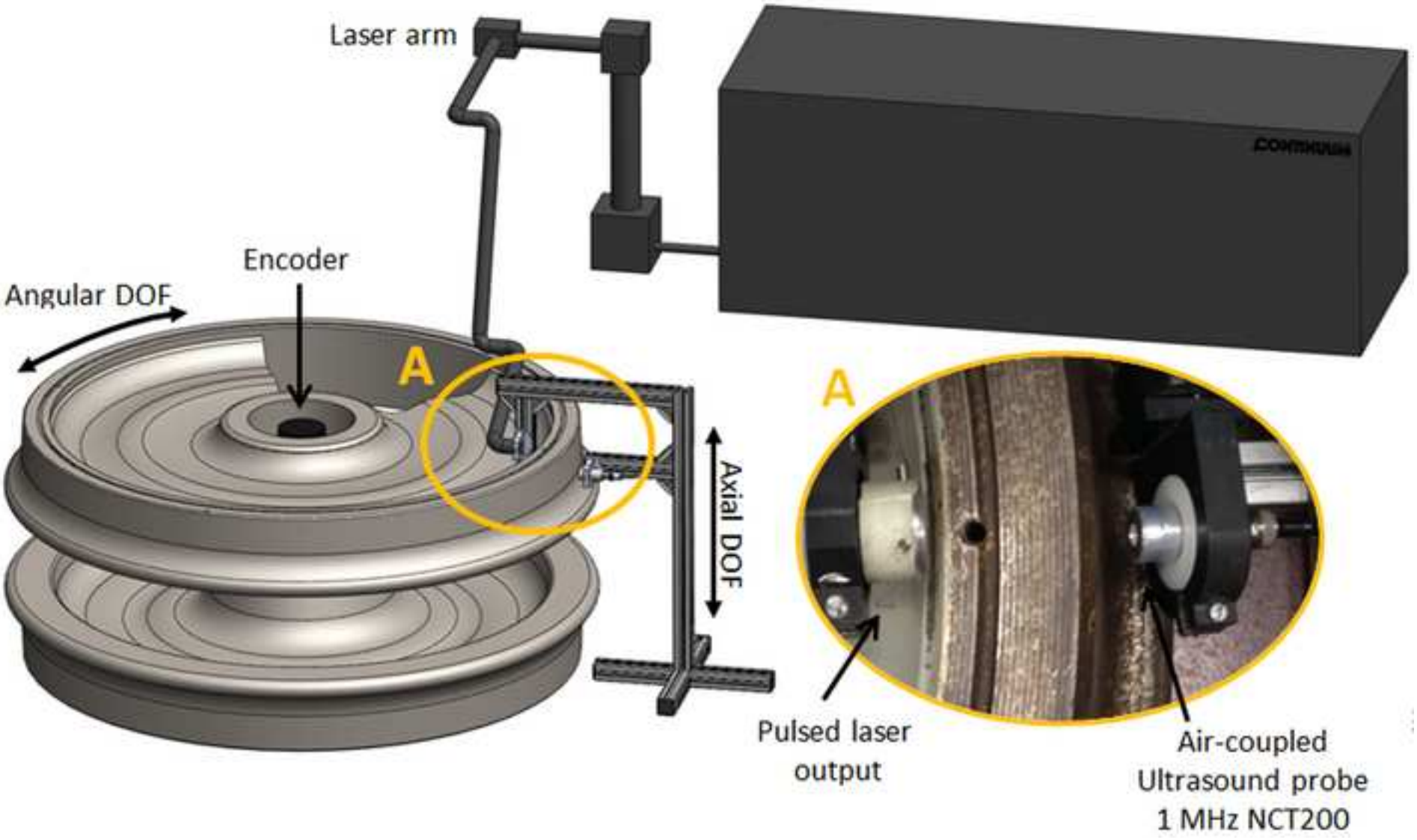

Fig.5. Test item (a) and defects created on it (b and c)
Click here to download high resolution image

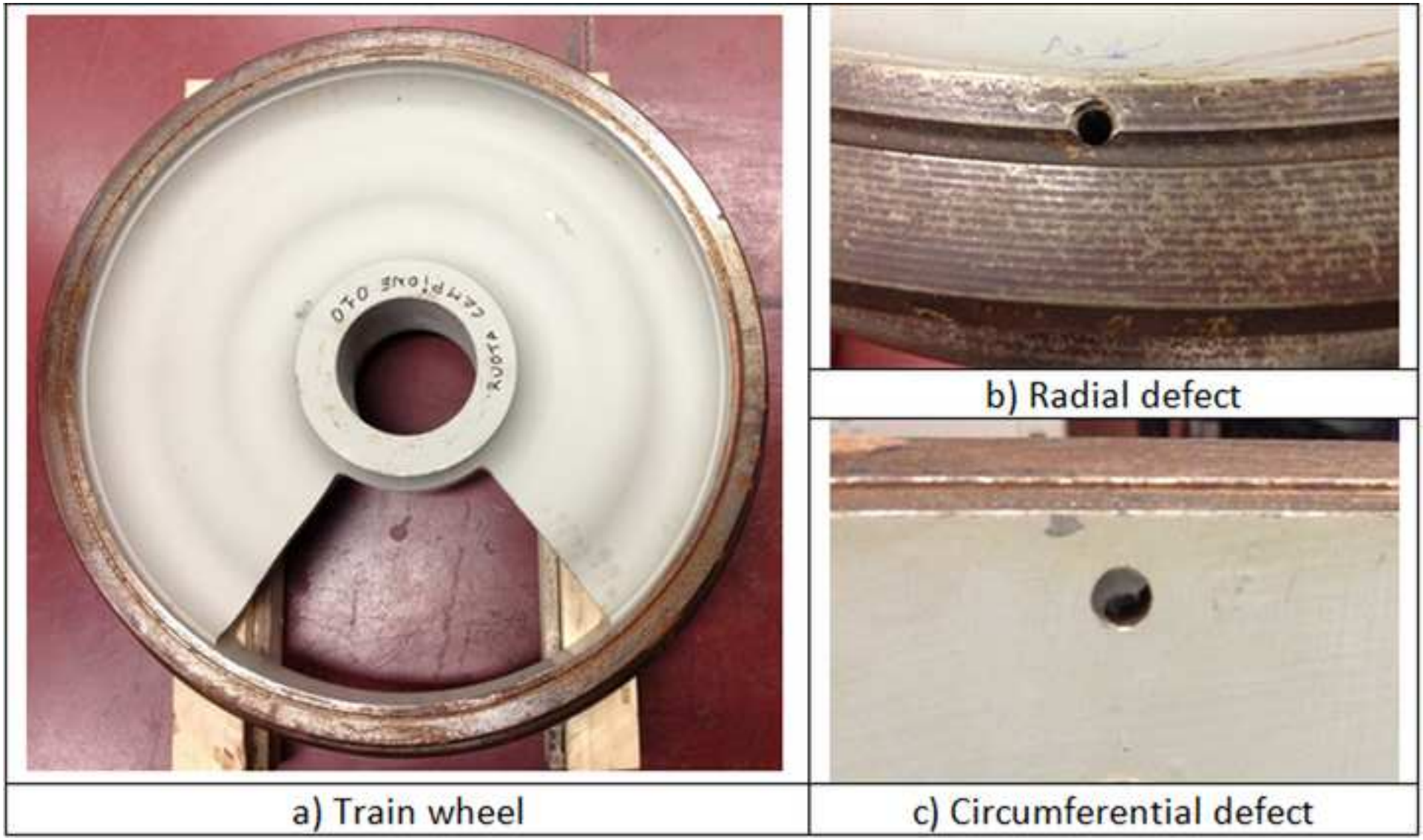

Fig. 6. US probe configuration and defect positions:
Click here to download high resolution image

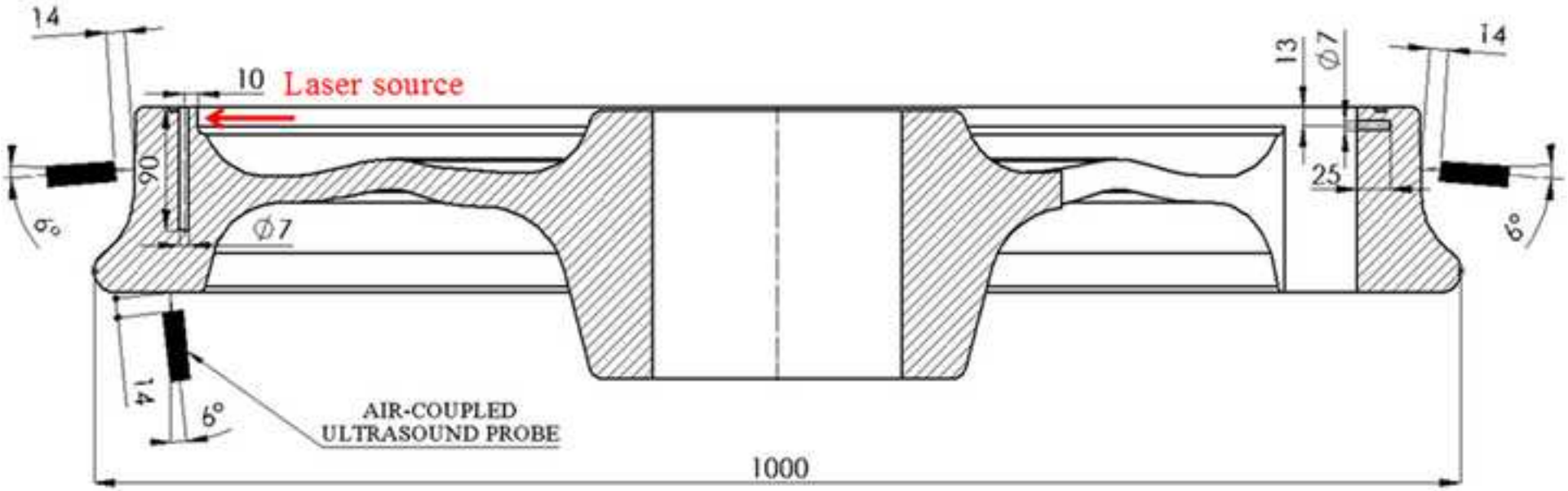

Fig. 7 Superposition of experimental

Click here to download high resolution image

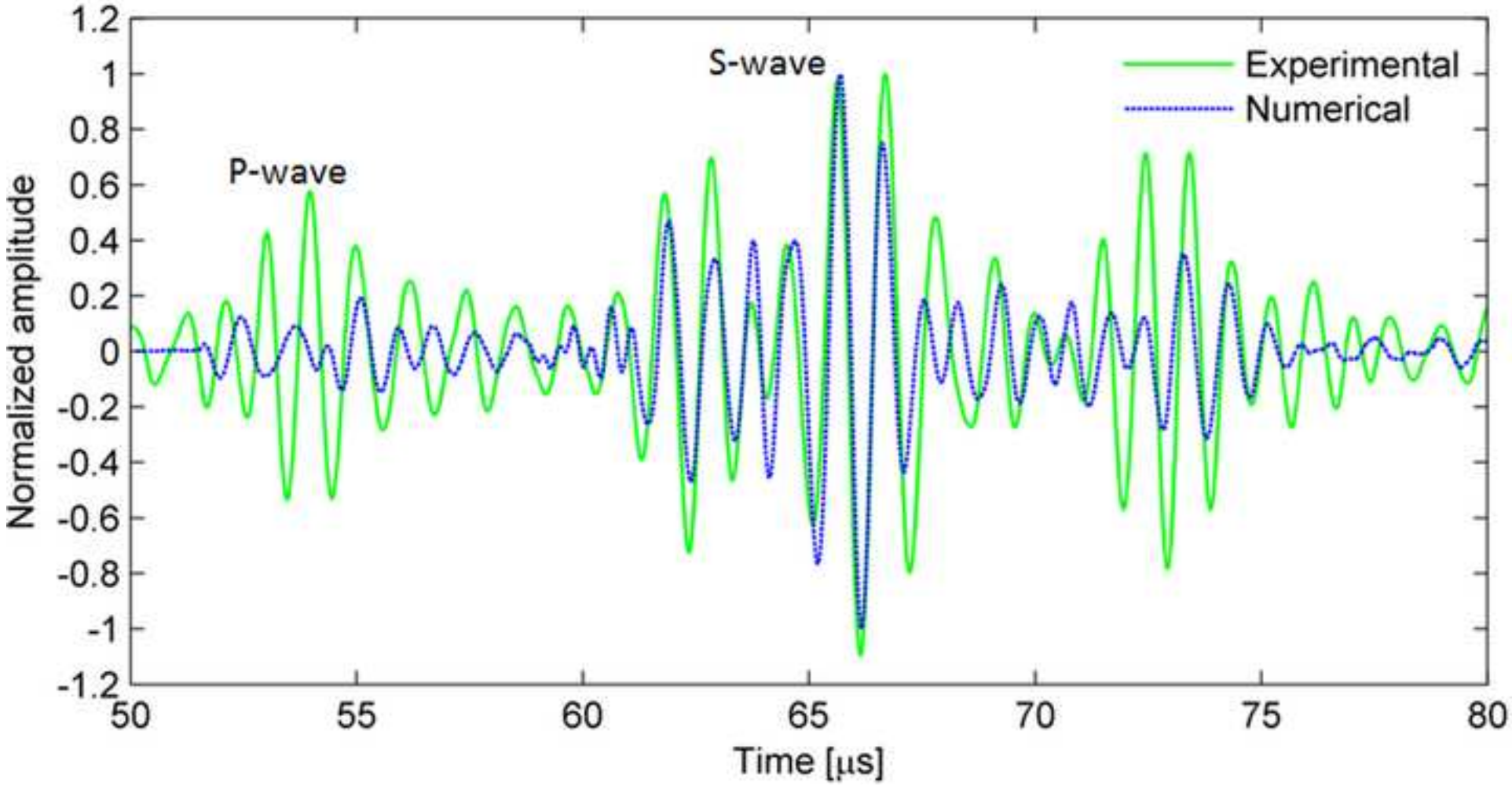

Fig. 8. Superposition of experimental

Click here to download high resolution image

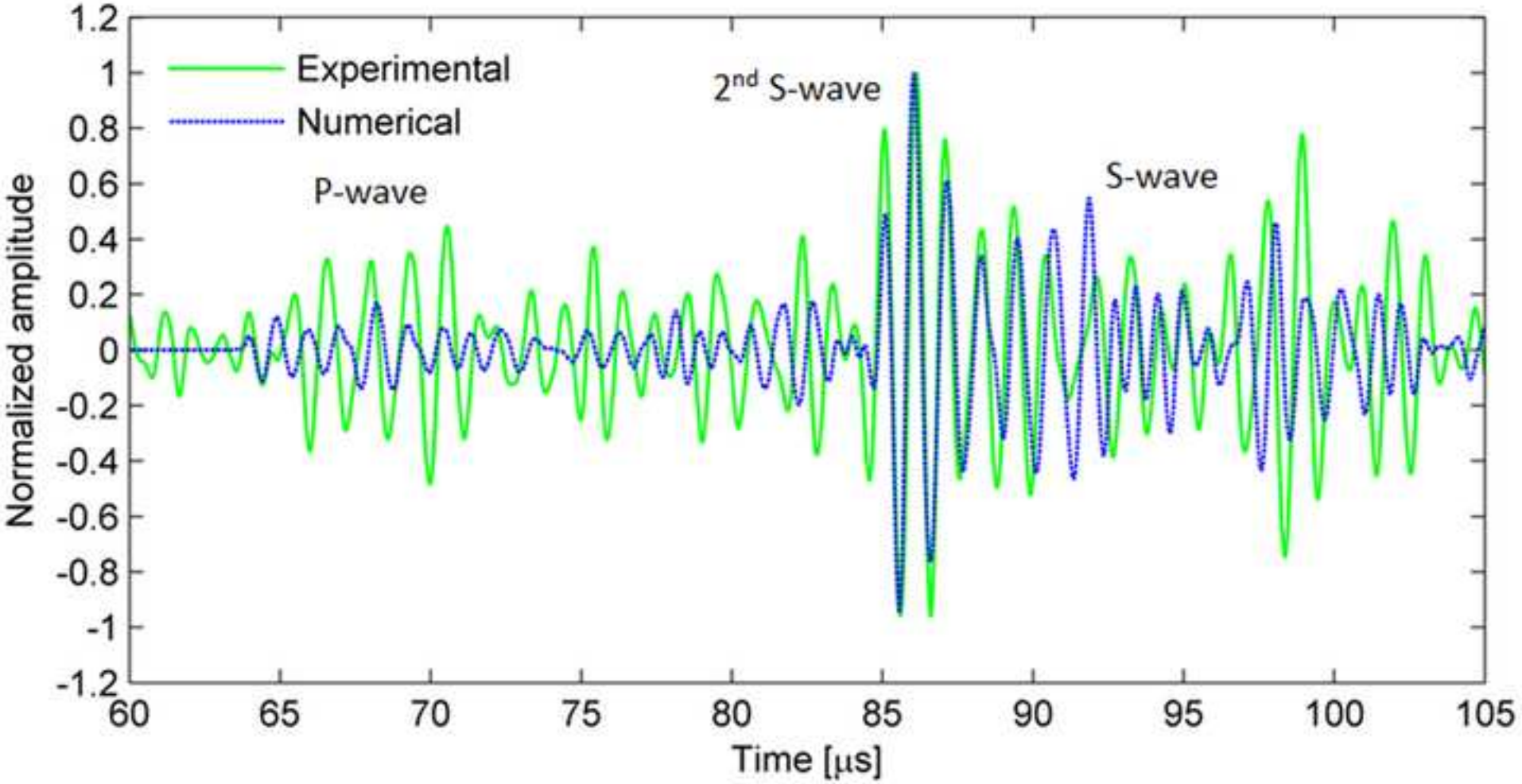

Fig. 9. Left: US probe in point 14, left column
Click here to download high resolution image

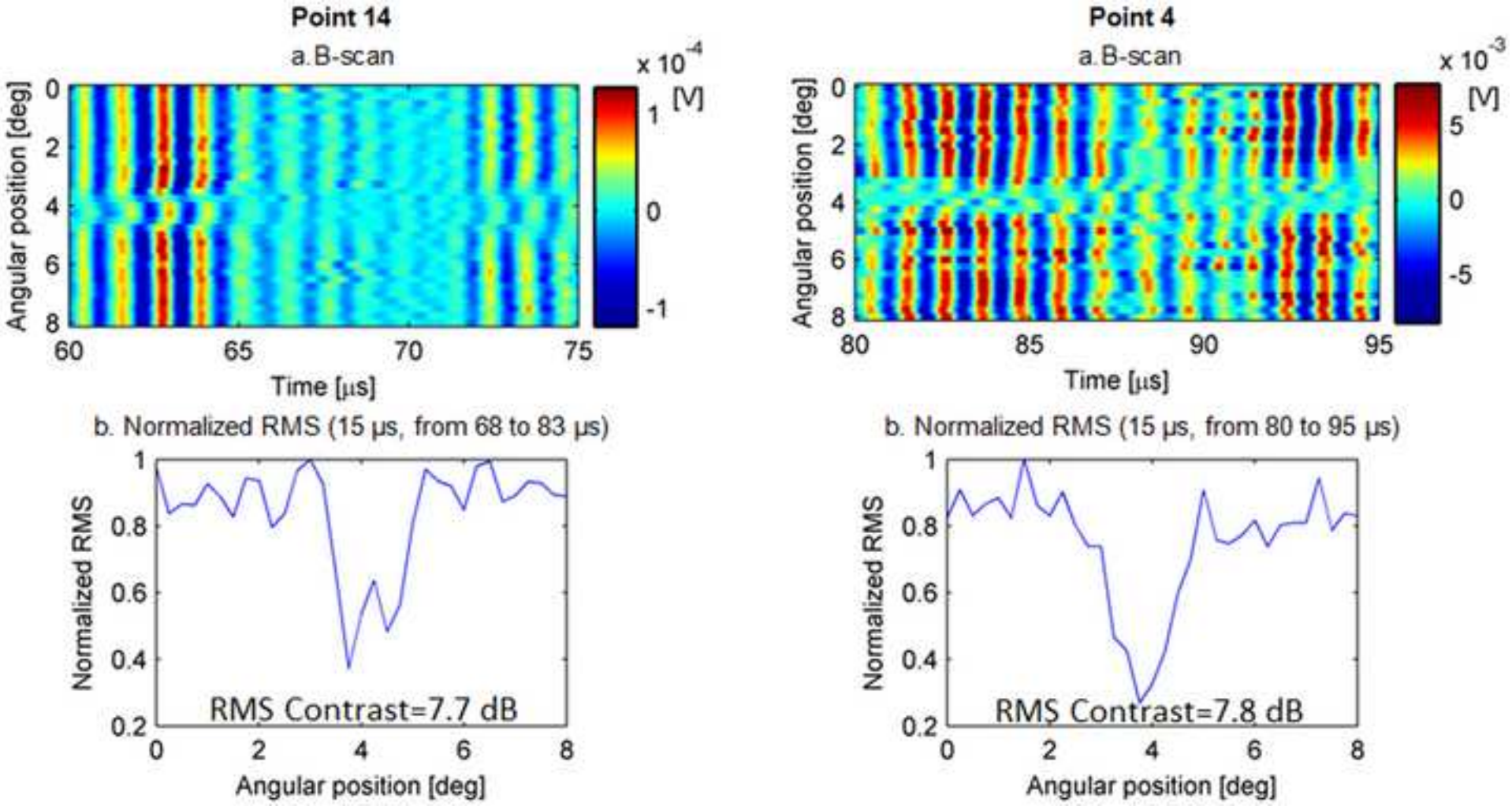

Fig. 10. US probe in point 14, B-scan
Click here to download high resolution image